ACS APPLIED MATERIALS & INTERFACES

Research Article

www.acsami.org

Microwrinkled Conducting Polymer Interface for Anisotropic Multicellular Alignment

Francesco Greco,*[,†] Toshinori Fujie,[†,‡] Leonardo Ricotti,[†,§] Silvia Taccola,[†] Barbara Mazzolai,[†] and Virgilio Mattoli[†]

[†]Center for MicroBioRobotics @SSSA, Istituto Italiano di Tecnologia, Viale Rinaldo Piaggio 34, 56025 Pontedera, Italy

[‡]European Biomedical Science Institute (EBSI), Organization for European Studies, Waseda University, 2-2 Wakamtsu-cho, Shinjuku, Tokyo 162-8480, Japan

[§]The BioRobotics Institute, Scuola Superiore Sant'Anna, Viale Rinaldo Piaggio 34, 56025 Pontedera, Italy

Supporting Information

ABSTRACT: Surfaces with controlled micro and nanoscale topographical cues are useful as smart scaffolds and biointerfaces for cell culture. Recently, use of thin-film and surface wrinkling is emerging as a rapid unconventional method for preparing topographically patterned surfaces, especially suited for the production of smart patterns over large area surfaces. On the other hand, there is an increasing interest in employing conducting polymers as soft, biocompatible, conductive biointerfaces or as parts of bioelectronic devices. A novel convenient and versatile method is presented for producing anisotropic topographical cues at the micro- and nanoscale on conducting polymer surfaces. Micro and nanowrinkles were formed during the heat-shrinking process of a thermo-retractable polystyrene substrate. Surface wrinkling was due to the mismatch between the mechanical properties of a conducting polymer ultrathin film and the substrate. Various geometries of wrinkled structures were prepared, demonstrating the tunability of topography depending on the thickness of the conductive film. A method for patterning the conductive properties of the wrinkled substrates was also presented. Such surfaces acted as smart scaffolds for the functional alignment of cells, envisioning their electrical stimulation. Cell adhesion and proliferation were evaluated, comparing different topographies, and a preferential anisotropic alignment of C2C12 murine skeletal muscle cells along wrinkles was demonstrated. The observed trends were also confirmed concerning the formation of aligned myotubes in C2C12 differentiation stage. Furthermore, improved results in terms of aligned and mature myotube formation were obtained by co-culturing C2C12 cells with a fibroblasts feeder layer. The combination of living cells and tunable conductive nanowrinkles will represent a unique tool for the development of innovative biomedical devices.

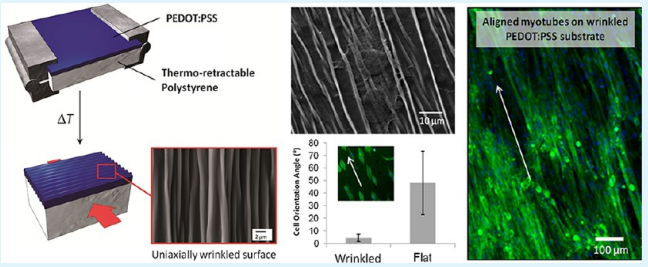

KEYWORDS: *smart biointerfaces, conducting polymer, surface wrinkling, cell alignment, biomimetics*

INTRODUCTION

The development of surfaces with controlled topographical cues at the micro- and nanoscale is of great importance for the fabrication of smart scaffolds and biointerfaces applied to in vitro cell culture and stimulation. One of the main challenges in this field is to mimic the in vivo features of extracellular matrix (ECM) and to provide the same mechano-transductive cues that influence many cellular functions. The effects of surface topography and in general of the surrounding microenvironment properties at the micro- and nanoscale on cell functions have been studied both on naturally occurring nanotopographic structures and on synthetic substrates with controlled topographical features. These studies permitted a better understanding of cell-material interactions and of contact guidance phenomena, in which substrate features at the micro- and nanoscales influence cell alignment, local migration, cell polarization, organelle formation, and so forth.[1] Cell responses to biophysical cues and, more specifically, to substrate topography, strongly depend on the chemico-physical properties of the substrate itself (e.g., stiffness), on feature sizes and geometries, and on cell types.[2−7]

The ability to control cell alignment, differentiation, and even fate through the use of topographically patterned substrates[8] has opened the way to major improvements in basic cell biology knowledge and to many applications in regenerative medicine and tissue engineering.[9,10] Topographically patterned surfaces at the micro and nanoscale have been obtained up to date by using inherently complex clean-room technologies, traditionally related to semiconductor industry. This allowed for fabricating substrates for cell culture with a very precise control of topography, though with simple periodic and homogeneous micro- and nanofeatures. Typically, grooved

Received: September 6, 2012
Accepted: December 28, 2012
Published: December 28, 2012

patterns are directly obtained on glass, silicon, and quartz by means of traditional microfabrication techniques, which also allow a precise patterning of various biodegradable polymers and elastomers by replica molding.[4,11] Substrates prepared through such approaches do not properly resemble native cell environments (i.e., ECM), as they are unable to mimic the multiscale arrangement of collagen fibrils, which provide topographical cues across a wide range of sizes. ECM shows a rather broad distribution of multiscale features rather than a precisely repeated, periodic array of cues.[12,13] Despite the recent availability of advanced methods for achieving multiscale topographies on substrates, by means of modified microfabrication techniques[14] or also by introducing some kind of nanoscale disorder,[15] their inherent complexity and the correspondent required cost, expertise, and equipment prevent their accessibility to a wider community of researchers and laboratories.

Conversely, thin-film and surface wrinkling is recently emerging as a rapid, inexpensive, unconventional method for surface patterning, especially suited for the production of smart patterns over large area surfaces and also for producing multiscale topographical features.[16,17] This mechanical instability-driven phenomenon of self-organization, widely observed in natural systems such as human skin or plants, is attracting more and more interest in the past years. Recently, some studies appeared about wrinkle formation induced by releasing a preimposed strain in the thin, stiff "skin" of an oxidized poly(dimethylsiloxane) (PDMS) surface and provided a model for the physical mechanism governing this process. In particular, nested, self-similar hierarchical patterns over various length scales have been obtained and characterized in the case of uniaxial or biaxial strain release.[18−20] On the other hand, surface wrinkling is gaining interest for its application in patterning engineered systems and artificial biomimetic materials.[16,21,22] Surface wrinkling indeed allows for relatively easy fabrication of well-defined and complex homogeneous topological features over very large areas. Very recently, biomimetic microwrinkled surfaces made of prestressed polyethylene (PE) have been tested as cell culture substrates for the functional alignment of human embryonic stem cell (hESC)-derived cardiomyocytes.[23] Similarly, stem cell morphology and differentiation have been recently controlled by culturing human mesenchymal stem cells (hMSCs) on the spontaneously formed wrinkled surface of a poly(2-hydroxyethyl methacrylate) (PHEMA) hydrogel prepared by a replica molding technique.[24]

On the other hand, there is an increasing interest in using conducting polymers (CPs) as soft, biocompatible, conductive biointerfaces or as parts of bioelectronic devices.[25,26] Indeed, when realizing CP-based electrodes or scaffolds, in addition to the electroconductive properties useful for applying electric fields or currents to biological samples, other interesting features can be added, such as controlled drug release, electromechanical stimulation, reversible electrochemical switching of surfaces for cell attachment/detachment, and so forth.[27−29] These applications are based on the peculiar properties of CPs as ionic conductors and electroactive materials.[25,30] In this sense, CPs represent a promising option toward the development of multifunctional smart biointerfaces, especially in the field of tissue engineering.[31,32] Among the different CPs, poly(3,4-ethylenedioxythiophene):poly(styrene sulfonate) (PEDOT:PSS) has been tested in many of the previously mentioned applications, and it is, in many cases, the material of choice because of its good stability, biocompatibility, ease of use, and availability on the market as an aqueous dispersion in a complete range of formulations for selected applications.[25−29]

The combination of living cells and tunable conductive nanowrinkles has the potential of constituting a unique tool for the development of innovative biomedical devices. Conductive properties of the substrate are actually requested for driving or boosting cell functions by using electrical stimulation[33] and the combined effects of 3D structure, surface topography, and conductive properties of scaffolds are recognized as crucial for the development of smart biointerfaces.[34] Moreover, the already cited dynamic and fully reversible eletroactive properties of conjugated polymers (e.g., the reversible electrochemical switching and the electromechanical actuation)[25,27−29] could open the way to the development of dynamic patterns and to tunable control of surface conductivity in situ. There is an increasing interest in developing dynamic patterns for cell culturing and only a limited number of topographical substrates with dynamic properties have been reported, at present. Most of them deal with a dynamic topographical control of cultured cells triggered by temperature, for example, by employing shape-memory polymers (SMP)[35,36] or stimuli-responsive hydrogels[37] with activation of the shape-memory effect (deswelling, in the case of hydrogels) near physiological temperature, that is, T = 37 °C.

With the aim of providing a convenient and versatile method for combining the good functional properties of conducting polymers with the ability of creating a defined topographic surface patterning, we prepared and characterized microwrinkled conductive polymeric surfaces based on thermoretractable polystyrene and PEDOT:PSS. By following a recent approach for the fabrication of wrinkled metal surfaces,[22] we deposited a conducting polymer film with submicrometric thickness on a thermo-retractable polystyrene sheet (commercially available as PolyShrink) by spin-coating an aqueous dispersion of PEDOT:PSS. A subsequent thermal treatment determined the substrate shrinking, while causing the buckling of the upper PEDOT:PSS layer, due to compressive stress. Anisotropically oriented micro- and nanowrinkles with various sizes and shapes were formed, depending on the fabrication procedure: biaxial wrinkles were formed on free-standing samples, while aligned uniaxial ones were fabricated by clamping two edges of the samples during shrinking.

After a thorough characterization of the conductive substrates obtained by means of such technique by SEM and AFM imaging and by four probe resistivity measurement, we investigated the adhesion, proliferation, and differentiation of murine skeletal muscle cells (C2C12) on the fabricated substrates, comparing samples with different topological features and assessing their influence on cell functions. Finally, a method for patterning the conductive properties of the wrinkled surfaces was tested, thus highlighting the possibility to draw individually addressable electrodes on the matrix surface and to dynamically control the electroactive properties of the conducting polymer. As a first proof of concept, cell adhesion was evaluated on samples with a simple line pattern that divided the surface into two adjacent electrodes and on biased samples, demonstrating cell patterning capability controlled by changing the electrochemical state of the surface.

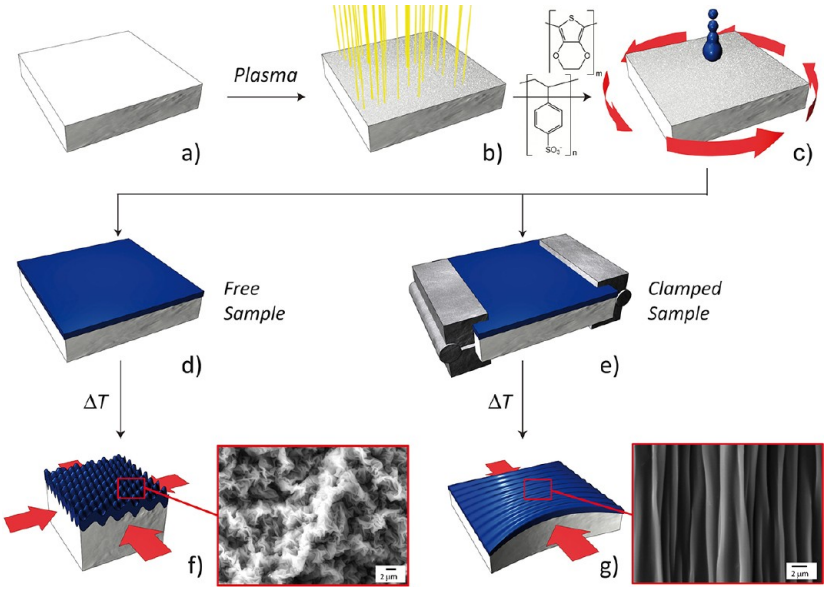

Figure 1. Schematic drawing of the process used for the fabrication of microwrinkled conductive surfaces: (a) thermo-retractable polystyrene sheet used as substrate; (b) air plasma treatment; (c) spin coating of PEDOT:PSS aqueous dispersion. Fabrication of (d,f) biaxially or (e,g) uniaxially wrinkled samples due to substrate shrinking caused by thermal treatment (T = 160 °C, 6 min). Red arrows in (f,g) show the directions of compressive stress acting on PEDOT:PSS layer during substrate shrinking. SEM pictures of the actual surfaces obtained in biaxially and uniaxially wrinkled samples are also shown in (f) and (g), respectively.

EXPERIMENTAL SECTION

Fabrication of Microwrinkled Conductive Polymeric Substrates. Thermo-retractable polystyrene sheets (PolyShrink) were purchased from Lucky Squirrel. PEDOT:PSS aqueous dispersion (Clevios P AG, H.C. Starck GmbH, Leverkusen, Germany) was used after filtration. The process is schematically described in Figure 1. PolyShrink foils (thickness, t = 200 μm) were cut in squares (2.5 × 2.5 cm^2), rinsed with deionized (DI) water, and dried with an air stream. To increase the surface wettability an air plasma treatment was provided (6.8 W, 80 s; Harrick PDC-002 Plasma Cleaner, Harrick Plasma). PEDOT:PSS was spin-coated on the polystyrene substrates by using different spin-coating speeds (s = 1000, 2000, and 3000 rounds per minute (rpm), respectively) for 60 s, to obtain films with different thicknesses, and allowed to dry at room temperature for at least 30 min before further processing. The thickness of the deposited PEDOT:PSS layer was evaluated on flat silicon substrates as described elsewhere.[38] Samples with different micro- and nanowrinkled surface topographies were obtained by operating a thermal treatment at T = 160 °C for 6 min, thus causing the shrinking of PolyShrink substrates to 40% of their original dimensions on surface x, y directions, while increasing their thickness (z direction; final thickness, t ∼ 2 mm). At the same time, such thermal treatment allowed a complete drying of the conductive film and a rearrangement of the PEDOT and PSS domains, making the film resistant to water, as already reported elsewhere.[38]

Different topographies were obtained depending on whether shrinking along both x, y directions (biaxial, B) or x direction (uniaxial, U) was permitted. Samples with formation of biaxial wrinkles were prepared by operating the thermal treatment on free-standing samples (samples B1, B2, B3, corresponding to spin coating speed s = 1000, 2000, and 3000 rpm, respectively, Figure 1.d, f). Conversely, uniaxial wrinkles were produced by clamping two edges of the sample, thus allowing the shrinking along x direction only (samples U1, U2, U3, corresponding to spin coating speed s = 1000, 2000, and 3000 rpm, respectively, Figure 1.e, g). Control flat samples for cell cultures were fabricated by spin-coating PEDOT:PSS on silicon wafer, keeping the same spin-coating speeds and operating the same heat treatment. Control flat samples for surface conductivity assessment were fabricated by spin-coating PEDOT:PSS with the same procedure on already shrunk Polyshrink samples of the same final size and drying them at T = 160 °C for 6 min (samples F1, F2, F3).

Patterned wrinkled samples U3p and patterned flat samples F3p of the same dimensions were prepared by patterning the conductive surface and subdividing it into two individually addressable electrodes, separated by a gap of width ∼500 μm. Patterning was realized by locally overoxidizing PEDOT:PSS with a sodium hypochlorite solution that caused the localized and irreversible loss of its conductive properties. In particular, a filter paper strip (laser cut, dimensions 12 × 0.45 mm) was soaked with a 10 wt % sodium hypochlorite solution in water (Sigma Aldrich), the excess liquid was gently removed, and the paper strip was put in contact with PEDOT:PSS surface for 30 s, with perpendicular direction to wrinkles alignment. Wet paper was able to conform and adhere to the wrinkled surface for the necessary time. The paper was then removed, the sample was immersed in DI water, and rinsed repeatedly to remove salt residuals. The sample was then dried by means of a nitrogen gun.

Surface Characterization. The surface topography of the self-organized wrinkled samples was characterized by means of scanning electron microscope (SEM) and atomic force microscope (AFM) imaging on as prepared samples. SEM images were obtained by using a EVO MA15 SEM (Zeiss, Germany) equipped with LaB_6 source and working at a 10 kV accelerating voltage. AFM scansions were performed using a Veeco Innova Scanning Probe Microscope (Veeco, USA). Measurements were performed in air, at room temperature, and operating in tapping mode, with oxide-sharpened silicon probes (RTESPA-CP) at a resonant frequency of ∼300 kHz. AFM images were processed for extracting information on wrinkle features with the aid of software analysis carried out by using Gwyddion SPM analysis tool and Origin Pro 8.1 (OriginLab, U.S.A.). Wrinkle periodicity was described by means of wavelength (distance between first neighbor peaks along the x axis) and height (height of individual peaks along the z axis), as obtained by considering the sequence of peaks in AFM profiles over 50 μm-long scansions along x axis (i.e., the direction perpendicular to the wrinkles). Peak positions and heights in each scansion were extracted semiautomatically by using the peak analyzer tool of Origin Pro 8.1 (peak finding and filtering by height imposing a 5% height threshold). To draw some statistical conclusions, measures were carried out over three different line profiles for each AFM image, considering three AFM images for each sample; three samples for each surface type (U1, U2, U3) were analyzed.

Surface Conductivity Assessment. The sheet resistance R_s of the different samples was evaluated by using a homemade four probe apparatus. A four probe head (JANDEL Engineering Ltd., U.K.) equipped with four retractable tungsten carbide tips was mounted on an *x, y, z,* and *q* manual micropositioning system (Melles Griot). The two external tips were connected to a galvanostat (Mod. 7050, AMEL, Italy) that permitted the controlled flow of a current $i = 2\ \mu$A. The two internal tips were connected to a voltmeter, measuring the voltage V, and the sheet resistance R_s was calculated by using the formula $R_s = \pi/\ln 2\ (V/i)$.[38]

Fibronectin Adsorption, Cell Cultures, and Co-Cultures. Uniaxially wrinkled samples (U1, U2, and U3) prepared as described above were cut into small pieces (1.0 × 1.0 cm^2) and subsequently used for cell culture. As control samples, flat substrates were prepared by spin-coating PEDOT:PSS at 3000 rpm on SiO_2 substrates. Before cell seeding, all specimens (three for each sample type, for each experiment) were sterilized by immersing them in a streptomycin solution (2 mg/mL in phosphate buffered saline, PBS) for 30 min. Nanowrinkled and control flat substrates were then treated with an air plasma (6.8 W, 45 s), and coated with 100 μg/mL fibronectin (Fn, Sigma-Aldrich), incubating the samples at 37 °C for 1 h to improve substrate cytophilicity. Conductive properties of samples were slightly affected by plasma treatment with an increase of ∼6% of electrical resistance in flat and wrinkled samples. Surface topography of the samples was not relevantly affected by the Fn coating, as evidenced by comparing AFM images of Fn-coated samples with those of pristine samples. To characterize the adsorption of Fn on the different sample surfaces, TRITC-Fn and FITC-Fn (Invitrogen), showing intense red and green fluorescence, respectively, were employed, keeping the same experimental conditions. After gentle rinsing the surface with PBS, samples were placed in cell growth medium, constituted by 90% Dulbecco's modified Eagle's medium (DMEM, Sigma-Aldrich) and 10% fetal bovine serum (FBS, ATCC), supplemented with 100 IU/ml penicillin, 100 μg/mL streptomycin and 2 mM L-glutamine. After 30 min, cells were seeded on the sample surface.

C2C12 were supplied from ATCC (passage <10). Cell densities were set as 15,000 cells/cm^2 for cell adhesion and proliferation studies, and 100,000 cells/cm^2 for differentiation studies, respectively. Concerning cell adhesion and proliferation experiments, C2C12 were kept in growth medium for 24 h and 72 h, respectively. Concerning differentiation experiments, C2C12 were kept for 24 h in growth medium after seeding, then the growth medium was replaced with differentiation medium, constituted by 98% DMEM, 1% FBS, and 1% Insulin-Transferrin-Sodium Selenite (ITS, Sigma-Aldrich),[39] and the cells were subsequently cultured for further 7 days, replacing the medium daily. Normal human dermal fibroblasts (nHDFs) were supplied from Lonza (passage <20) and were used as feeder layer for C2C12 cells, to enhance their differentiation toward the skeletal muscle phenotype. nHDFs were seeded on sample surfaces with a density of 10,000 cells/cm^2 and kept for 24 h in growth medium (with the same formulation used for C2C12 cells). The cells were then treated with 10 μg/mL mitomycin C (Sigma-Aldrich) in growth medium and incubated at 37 °C for 2 h, to inactivate fibroblast mitotic activity and to provide a suitable feeder layer. After this step, samples were rinsed with PBS and provided with fresh growth medium. C2C12 cells were then seeded on top of the fibroblast layer with a density of 100,000 cells/cm^2. Such co-culture was kept in a growth medium for 24 h, then shifted toward a differentiation medium, and maintained for further 7 days, replacing the medium daily.

Cell Proliferation Assessment. C2C12 proliferation was quantitatively evaluated after 24 and 72 h of culture, by means of double-stranded (ds)-DNA quantification. Briefly, the culture medium was removed from the samples and double distilled water (dd)-H_2O was added. The samples were then immediately frozen at −20 °C and stored for subsequent assays. Cell lysates were obtained by two freeze/thaw cycles of the samples. Ds-DNA content in cell lysates was measured using the PicoGreen kit (Molecular Probes). The PicoGreen dye binds to ds-DNA and the resulting fluorescence intensity is directly proportional to the ds-DNA concentration in solution. Working buffer and PicoGreen dye solutions were prepared according to the manufacturer's instructions and were added (100 and 150 μL, respectively) to each well. After 10 min of incubation at room temperature in the dark, fluorescence intensity was measured on a plate reader (Victor3; PerkinElmer, Waltham, MA) using an excitation wavelength of 485 nm and an emission wavelength of 535 nm. The above-mentioned experiment was carried out in triplicate, using three samples for each substrate type and for each time-point.

Cell Fixation, Staining, and Extraction of Cell Shape-Related Parameters. Cells were fixed at two different end points (1 day and 7 days) for cell adhesion studies and cell differentiation studies, respectively. In both cases, we analyzed three samples for each substrate type, and the procedure for cell fixation, nuclei and cytoskeletal actin fluorescent staining was the following: at the end point, culture medium was removed, cells were rinsed with PBS and incubated with 3.7% paraformaldehyde in H_2O for 15 min. Standard procedures were then followed for staining. Oregon Green 488 phalloidin (Invitrogen, Carlsbad, CA) was used to stain F-actin and 1 μM DAPI was used to stain cell nuclei. The samples were then observed with an inverted fluorescent microscope (Eclipse Ti, FITC-TRITC-DAPI filters, Nikon, Melville, NY) equipped with a cooled CCD camera (DS-5MC USB2, Nikon) and with NIS Elements imaging software. For SEM analysis, the fixed cells were dehydrated with a graded ethanol series.

For cell adhesion studies, cell shape index and cell alignment along a preferential axis were quantified for the cells cultured on the different samples. Cell shape index (CSI) was calculated using the following formula: $CSI = 4\pi A/P^2$, where A and P were the area and the perimeter, respectively, of a cell. Such index is a measurement of how circular or linear an object is. It ranges from 0 to 1, and the larger the value of the shape index, the more round-shaped the cell is. Such parameter was extracted from fluorescence images (five 10× magnification images for each sample) by using the free image processing software ImageJ (National Institutes of Health, U.S.A.), available at http://rsbweb.nih.gov/ij/download.html. Cell alignment along a preferential axis was evaluated, using the same software, by measuring the angle that each cell's main axis formed with a preferential axis.

For cell differentiation studies, some myotube-related parameters were assessed. The fusion index was determined by dividing, for each picture, the total number of nuclei in myotubes (≥2 nuclei) by the total number of counted nuclei. Myotube length and width were extracted from each image using ImageJ. Myotube alignment was evaluated, using the same software, by measuring the angle that each myotube formed with a preferential axis. The closer the angle to 0°, the more the myotubes resulted aligned along a specific direction on the substrate; the closer the angle to 45°, the more the myotubes were randomly oriented on the substrate. As before, five 10× magnification images for each sample were analyzed.

Electrical Patterning of Cells on Conductive Substrates. Patterned substrates U3p and F3p prepared as described above with two adjacent electrode surfaces separated by an insulating gap were used for testing electrical patterning of cells. Two contact Au electrodes (1 × 1 mm^2) were first deposited on samples through physical masks, one on each separated electrode surface (Au deposition at 40 mA 120s, Q150R ES Sputter Coater, Quorum technologies, U.K.) and insulated copper wires were connected to electrodes with silver epoxy adhesive. Contacts were then sealed with electrically insulating varnish to prevent direct contact with electrolytes. Prior to cell seeding, all the substrates were treated with air plasma (6.8 W, 45 s) and incubated with a 100 μg/mL fibronectin solution at 37 °C for 1 h, then rinsed and placed in the culture medium. Immediately before cell seeding, samples were connected to 1.5 V AA batteries, with electrodes on the same sample connected to different polarity + or −, to, respectively, oxidize and reduce their distinct portions. nHDFs and C2C12 cells were then seeded at densities of 10,000 cells/cm^2 and 100,000 cells/cm^2, respectively (the same densities used for differentiation experiments) and cultured for 24 h, by keeping the electrical stimulus during the whole culture period. At the end of the 24 h end-point, batteries were disconnected,

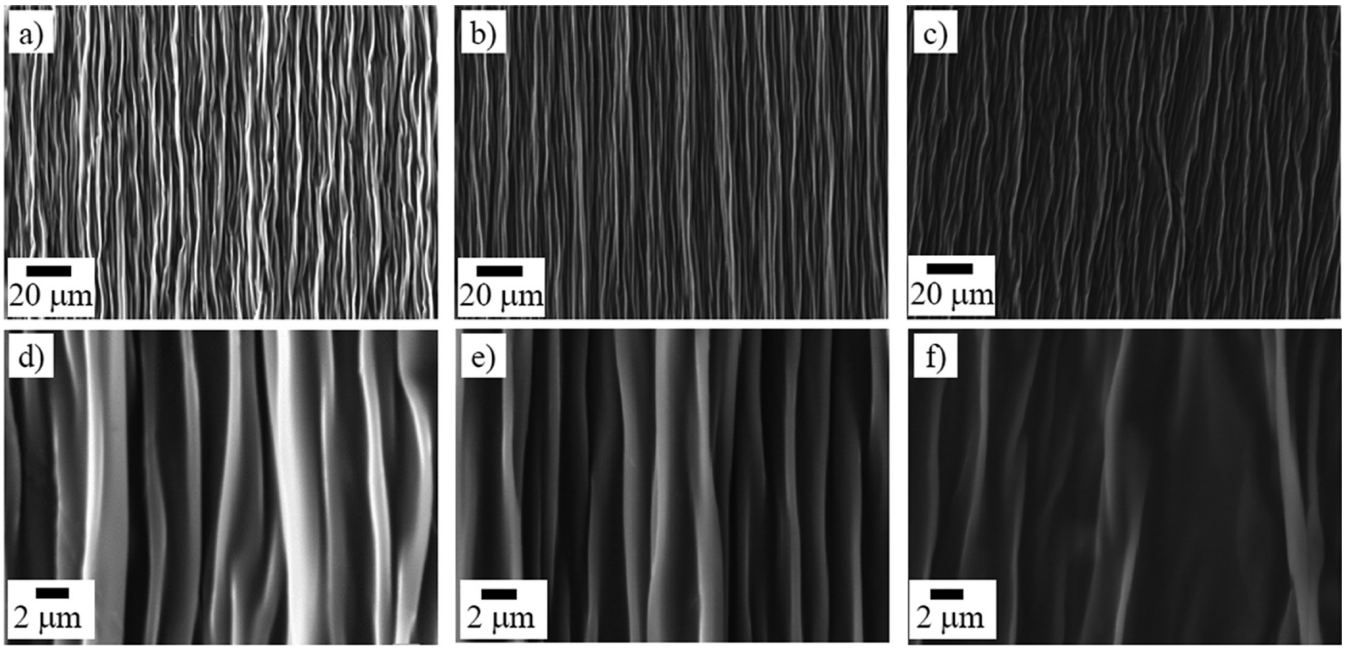

Figure 2. Low-magnification (a–c) and high-magnification (d–f) SEM images of uniaxially microwrinkled PEDOT:PSS surfaces obtained in the case of U1(a, d), U2 (b, e), and U3 (c, f) samples.

and cells were fixed, permeabilized, and stained for cell nuclei by means of 1 μM DAPI.

Statistical Analyses. Collected data underwent analysis of variance (ANOVA), for evaluating statistically significant differences among samples. *T*-test was performed in the case of comparison between two groups, while Holm-Sidak tests were performed in the case of comparison among more groups with $*p < 0.05$ and $**p < 0.01$ set as the levels of statistical significance.

RESULTS AND DISCUSSION

Characterization of Wrinkled Surfaces. Micro- and nanowrinkled conductive scaffolds were obtained with different geometries and feature sizes depending on the fabrication parameters. In Figure 1f, g, SEM micrographs show the peculiar surface topography obtained in the case of biaxial and uniaxial wrinkles, respectively. The spontaneous formation of surface wrinkling was due to the planar compressive forces acting on the thin, stiffer PEDOT:PSS layer attached to the prestressed polystyrene substrate that, upon heating, irreversibly shrunk to 40% of its original dimension, while increasing its thickness from 0.2 to ~2 mm. As a useful comparison, SEM pictures of the surface of pristine PolyShrink before thermal shrinking (without PEDOT:PSS coating), of uniaxially or biaxially shrinked PolyShrink (without PEDOT:PSS coating) and of flat (F3) sample (coated with PEDOT:PSS) are shown in Supporting Information, Figure S2. No wrinkling is evidenced in such samples.

The fabricated structures showed a high robustness, despite the nanoscale size of the conductive layer and of the topological features. Compressive forces acting on the top PEDOT:PSS layer during substrate shrinking were in fact not able to damage the film, that kept its continuity without ruptures over the whole surface in both cases (uniaxial and biaxial wrinkles formation). The wrinkled PEDOT:PSS layer was interlocked with the polystyrene substrate, because of structural penetration into the soft substrate during the heat-shrink process. Heating process was indeed performed at T = 160 °C, well above the glass transition temperature of polystyrene (T_g ~ 100 °C). This allowed for softening of the substrate during shrinking, thus relaxing excess tension. The Young's modulus of polystyrene at room temperature (i.e., 3.0–3.5 GPa), decreases more than 100 times (i.e., ~ 1 MPa) when it is heated beyond its T_g.[40] On the other hand, as we previously reported, the Young's modulus of PEDOT:PSS ultrathin films is around 1 GPa.[38] Once the sample was cooled at RT and the substrate restored its glass state, the formed wrinkles strongly adhered to the substrate because of good interlocking between PEDOT:PSS and polystyrene.

In the case of biaxially wrinkled samples (B), a complex surface topography with multiscale formation of wrinkles was observed, as clearly depicted in Figure 1f. Submicrometric wrinkles with sharp edges and extensive folding of the upper PEDOT:PSS layer were obtained. A pronounced surface waviness with periodicity of several micrometers was observed as well. This is more clearly evidenced in the Supporting Information, Figure S3a,b.

In the case of uniaxially wrinkled samples U, clamping along one direction during sample shrinking caused the formation of wrinkles with rounded shape, aligned along clamping direction (Figure 1.g). Topographic features of uniaxially wrinkled surfaces were tuned by varying the thickness t of the PEDOT:PSS layer. U1, U2, and U3 samples were then characterized by SEM and AFM imaging. Differences in surface topography depending on t were visible in micrographs reported in Figure 2 and in AFM scansions reported in Figure 3a–c. Table 1 summarizes the topological properties of U1, U2, and U3 samples in terms of wrinkle average wavelength λ and height h, as obtained by analyzing AFM scansions. As expected, spatial wrinkle periodicity is affected by thickness, with λ and h both increasing with thickness t.[16]

The average values of λ and h reported in Table 1, while giving a synthetic description of the surface and of the observed differences among different samples types, do not fully reflect the richness of multiscale topological features observed in AFM scansions, as for example, those depicted in Figure 3a–c.

dx.doi.org/10.1021/am301908w | ACS Appl. Mater. Interfaces 2013, 5, 573–584

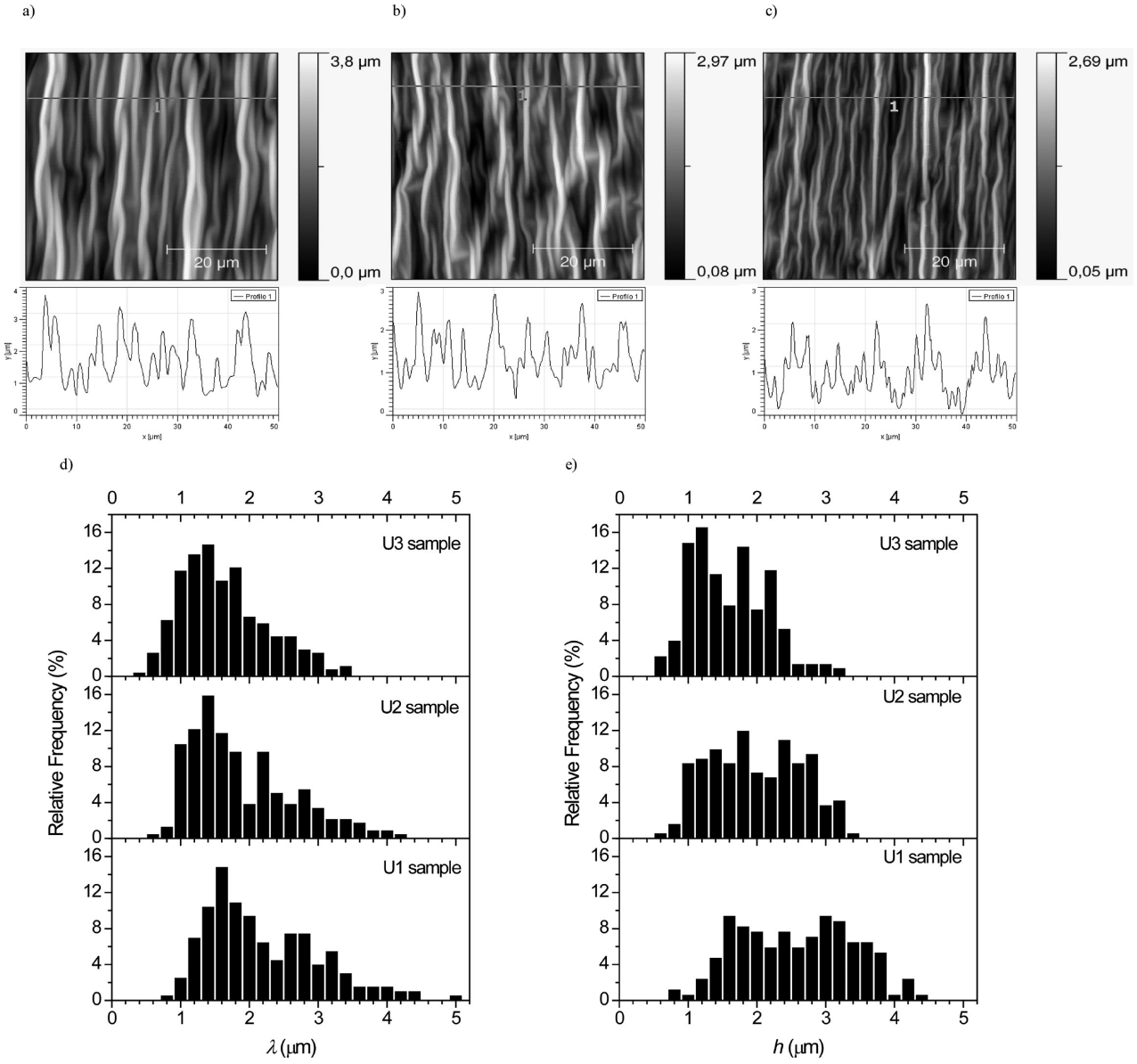

Figure 3. Top: AFM analysis (50 × 50 μm^2 areas) and corresponding line scan profiles of samples U1 (a), U2 (b), and U3 (c). Bottom: relative frequency distributions of wrinkle wavelength λ (d) and peak height h (e) as obtained by analyzing AFM images for U1, U2, and U3 samples.

Table 1. Topological Properties of Uniaxial Nano-Wrinkles[a]

sample	s (rpm)	t (nm)	λ (μm)	h (μm)
U1	1000	120.9 ± 1.5	1.95 ± 0.80	2.45 ± 0.82
U2	2000	78.6 ± 2.8	1.64 ± 0.73	1.84 ± 0.66
U3	3000	53.6 ± 1.2	1.56 ± 0.61	1.45 ± 0.55

[a]Obtained by changing PEDOT:PSS thickness: spin-coating speed s, PEDOT:PSS layer thickness t, wrinkles average wavelength λ, and wrinkles average height h are reported (as obtained by AFM imaging). Errors are given as standard deviations of the measured values. Concerning wavelength λ and height h, each sample type was statistically different from all the other ones with $p < 0.01$.

To give a deeper insight in these features, height profiles of several AFM scansions were considered for each different U sample, and the observed peaks were classified on the basis of their relative height and wavelength, thus obtaining the distributions of wrinkle λ and h depicted in Figure 3d, e. The coexistence of a rather broad range of wavelengths and peak heights for each sample was observed, with higher peaks, larger wavelengths, and wider distributions obtained for the thicker PEDOT:PSS layer in the series, namely, U1. Median values of the distributions as well as their width decreased with thickness while a bimodal distribution was probably emerging for U1 and U2. Moreover, the relative frequency of submicrometer features was markedly increased from U1 to U3 samples. While the spatial periodicity at small scales (0−5 μm) was well described by AFM scansion, by taking into account wrinkle wavelength λ, defined as the distance between nearest neighbor wrinkles, larger scale periodicity was totally neglected. The superposition of wrinkles at various scales better emerged from SEM images at lower magnification, as in the case of Figure 2a−c and Supporting Information, Figure S3.c, rather than in AFM scansions, because of their limitations in the maximum surface scanning area. The multiscale character of wrinkled surfaces and the observed broad distributions of topographic features show some similarities with naturally occurring microenvironment for cells (e.g., ECM), better mimicking it in comparison with ultra

precise and homogeneous scaffolds obtained by means of traditional microfabrication techniques. On the other hand, as visible in AFM scansions (Figure 3a–c), uniaxially aligned wrinkles in all the cases maintained a rounded and "smooth" shape, which is known to have a beneficial effect on contact guidance of philopodia attachment.[13]

Surface Conductivity Assessment. Conductive properties of the PEDOT:PSS layer were fully retained in shrunk samples, as confirmed by measurement of sheet resistance R_s performed on uniaxially and biaxially wrinkled samples.

Table 2 reports the sheet resistance values obtained in the case of uniaxially (U) and biaxially (B) wrinkled samples, as well as those obtained for control flat samples (F) with different PEDOT:PSS layer thicknesses. In the case of U samples, sheet resistance was measured parallel or perpendicularly with respect to wrinkle axis, obtaining different values ($R_{s\parallel}$ and $R_{s\perp}$, respectively), because of the anisotropy of the topological features.

Table 2. Sheet Resistance R_s of Samples with Flat (F) Biaxially Wrinkled (B) or Uniaxially Wrinkled (U) Surface for Different Thicknesses of the PEDOT:PSS Layer[a]

sample	s (rpm)	R_s (kΩ/sq)	$R_{s\parallel}$ (kΩ/sq)	$R_{s\perp}$ (kΩ/sq)
F1	1000	271 ± 13		
F2	2000	475 ± 13		
F3	3000	586 ± 16		
B1	1000	199 ± 11		
B2	2000	330 ± 9		
B3	3000	442 ± 20		
U1	1000		300 ± 13	348 ± 13
U2	2000		489 ± 11	538 ± 21
U3	3000		611 ± 20	681 ± 15

[a]In the case of U samples sheet resistance was measured along perpendicular direction ($R_{s\perp}$) and parallel direction ($R_{s\parallel}$) with respect to the wrinkle alignment direction. Errors are given as standard deviations of the measured values.

Sheet resistance consistently increased in all the F, B, and U series with decreasing the PEDOT:PSS layer thickness. As regards the uniaxially wrinkled samples, it was interesting to compare the obtained sheet resistance values with those observed for B and F samples with similar PEDOT:PSS thickness. Sheet resistance $R_{s\parallel}$ of U samples is only slightly larger with respect to R_s of flat control samples F (PEDOT:PSS spin-coated on already shrunk thermo-retractable polystyrene) accounting for very similar length of conductive pathways in both sample types. On the other hand, the larger $R_{s\perp}$ values are ascribable to an increase of the actual area of the uniaxially wrinkled surface. Thus, the actual length of conductive pathways between probes was larger in the case of uniaxial wrinkles with respect to flat sample showing the same geometrical size. Moreover, local cracks can sometime occur in the wrinkled conductive surface, thus slightly increasing the sheet resistance. As regards the differences observed between $R_{s\parallel}$ and $R_{s\perp}$ values, it is also interesting to notice that their ratio is not changing with the thickness of PEDOT:PSS, being almost stable in all the sample series: $R_{s\parallel}/R_{s\perp} \sim 0.88$. Such result is therefore due only to the shrinking of the sample along one direction and not to the surface topography (different periodicity of the wrinkles). Furthermore, in all the cases, biaxially wrinkled samples B showed reduced R_s values with respect to F and U samples. Neighbor wrinkle edges are actually in contact with each other in the biaxially wrinkled samples, as visible in the micrograph reported in Figure 1f and Supporting Information, Figure S3.a, b, thus allowing for establishing shorter conductive pathways and reduced sheet resistance with respect to the uniaxial or the flat case.

Fibronectin Adsorption, Cell Adhesion, Proliferation, and Alignment. Fn layer adsorption on the different samples was evaluated by fluorescence images of substrates treated with TRITC-Fn (Supporting Information, Figure S4.a). The images

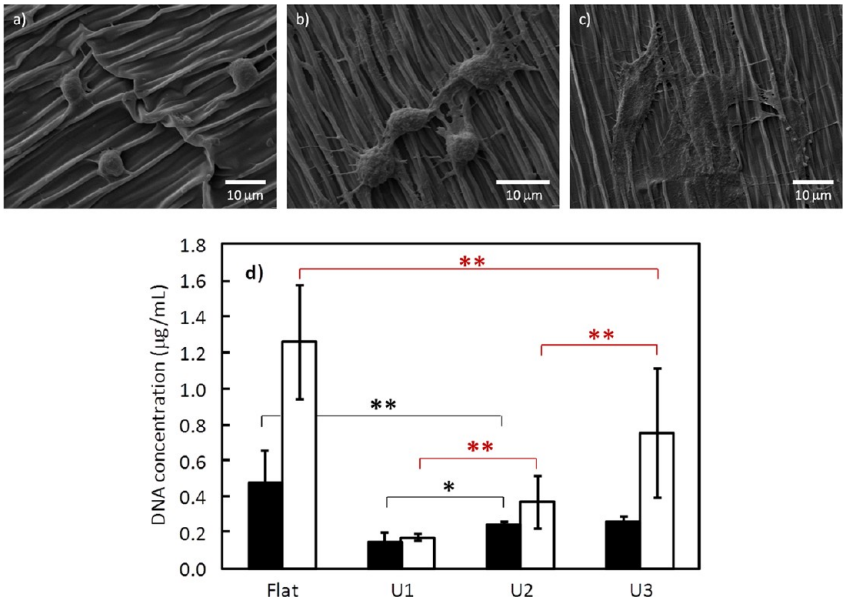

Figure 4. SEM morphological images of C2C12 cells adhered on the different nanowrinkled sample surfaces: U1 (a), U2 (b), and U3 (c). (d) Comparison of cell proliferation, assessed by means of DNA concentration, after 1 day (black bars) and 3 days (white bars). * = $p < 0.05$, ** = $p < 0.01$. Black lines refer to statistical comparisons between 24 h-cultured samples. Red lines refer to statistical comparisons between 72 h-cultured samples.

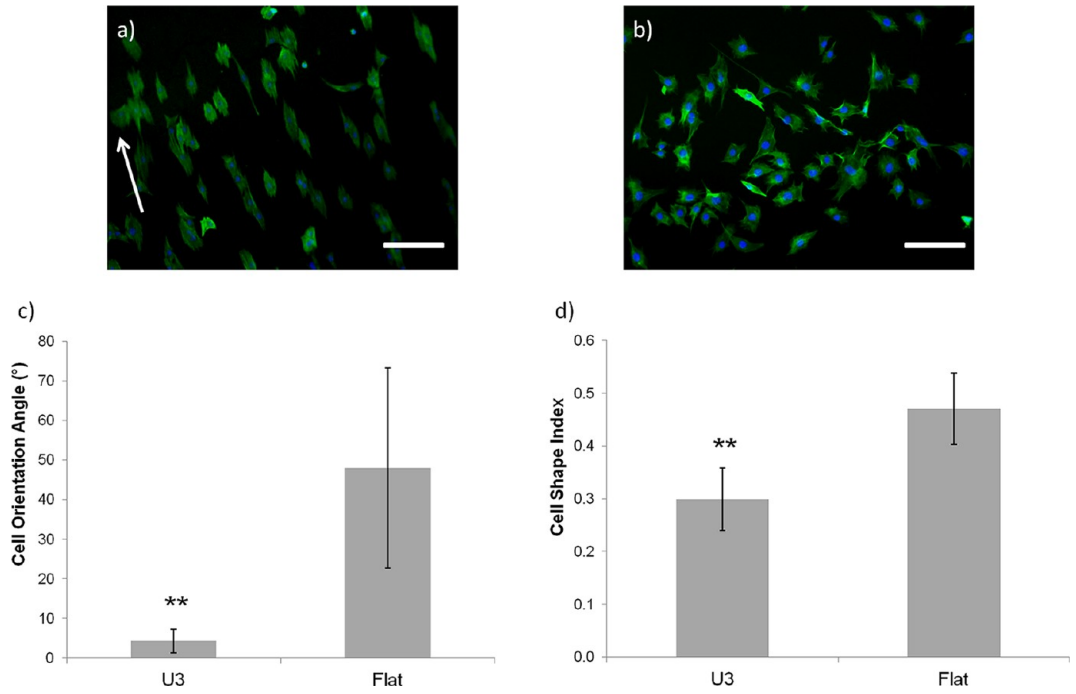

Figure 5. Comparison of adhesion properties of C2C12 cells cultured on U3 (a) and control flat substrate (b), visualized under the fluorescent microscope. White arrow shows the alignment direction of the nanowrinkles. Scale bar is 100 μm. Cell Orientation Angle (c) and Cell Shape Index (d) after 24 h of culture. ** = $p < 0.01$.

revealed a uniform protein coating on all the sample types, with no evidence of protein agglomeration. The Fn concentration used in this study (100 μg/mL) is rather high in comparison with the literature, reporting lower concentrations (~20 μg/mL) for scaffold treatment.[41] We observed that treating our samples with a "standard" concentration of Fn (e.g., 20 μg/mL) resulted in a rather poor cell adhesion (Supporting Information, Figure S4.b). This could be due to the sample geometry and to its handling procedure, causing a significant protein sliding from the sample and resulting in a reduced amount of Fn actually adsorbed on the sample surface.

C2C12 adhesion and proliferation were assessed for U1, U2, and U3 samples (Figure 4). To determine adhesion properties, cells were cultured for 24 h on the three scaffold types, then fixed and qualitatively analyzed by SEM imaging. Some differences are clearly visible in the morphology of cells adhered on the different scaffolds. Cells adhered on U1 and U2 substrates (Figure 4 a,b) showed a rounded, apoptotic shape, and were anchored to the ridges of the wrinkled surface with some filopodia of limited number and length. Individual cells were not able to spread over a large area and to span many ridges. Although very similar to U1, cell morphology on U2 substrates was maybe slightly better than that on U1 samples. On the other hand, cell morphology on U3 samples (Figure 4.c) was very different, since cells showed an almost flat shape and were able to spread over multiple ridges. Although qualitative, this comparison permitted to appreciate the differences in cell adhesion due to the change in surface topography: U3 topography, characterized by lower ridges with respect to U2 and U1, allows for a better cell adhesion and spreading.

Wrinkle dimensions also influenced cell proliferation (Figure 4d). C2C12 proliferation rate was higher for cells cultured on flat PEDOT:PSS substrates, in comparison with those cultured on U1, U2, and U3 samples. Concerning U1 and U2 samples, the reduced cell proliferation ability has to be attributed to the physical constraints determined by the high and wide wrinkle ridges of such samples, limiting cell ability to divide and spread. This effect plays a minor role for U3 samples, being cells able to spread well over the wrinkle ridges (Figure 4c). The reduced proliferation rate for cells cultured on U3 samples, in comparison with those cultured on control flat substrates, is consistent with previous literature evidence, highlighting that cells grown on grooves or wrinkles show a lower proliferative ability compared with cells grown on a flat surface.[42−45]

Cell alignment was evaluated by culturing C2C12 cells on flat PEDOT:PSS and U3 samples, by fixing them after 24 h of culture, by performing cytoskeletal immunostaining, and by quantifying cell alignment along a preferential axis (Figure 5). Cells cultured on nanowrinkled substrates showed a good alignment along the nanowrinkle axis (Figure 5.a), while those cultured on flat substrates showed an isotropic cytoskeletal organization (Figure 5.b). This result was confirmed by quantitative parameters extracted from fluorescence images, related to cell orientation angle (Figure 5.c) and Cell Shape Index (Figure 5.d).

As known, initial cell seeding density affects cell orientation.[46] For all the differentiation studies, the initial cell density was much higher (100.000 cells/cm^2) in comparison with the density used for cell alignment studies. The reasons of such high initial cell seeding density for differentiation studies were 2-fold: (i) to ensure cell confluence 24 h after cell seeding; (ii) to compensate cell sliding from the sample surface, due to sample handling procedures during cell seeding. To evaluate if the high cell density negatively affected cell alignment, we stained C2C12, seeded at 100.000 cells/cm^2 on flat and U3 substrates, after 24 h of culture. Results (Supporting Information, Figure S5) revealed that a confluent cell layer was achieved on both samples, with a clear (even if not easily quantifiable, due to cell crowding) cell isotropy on flat controls

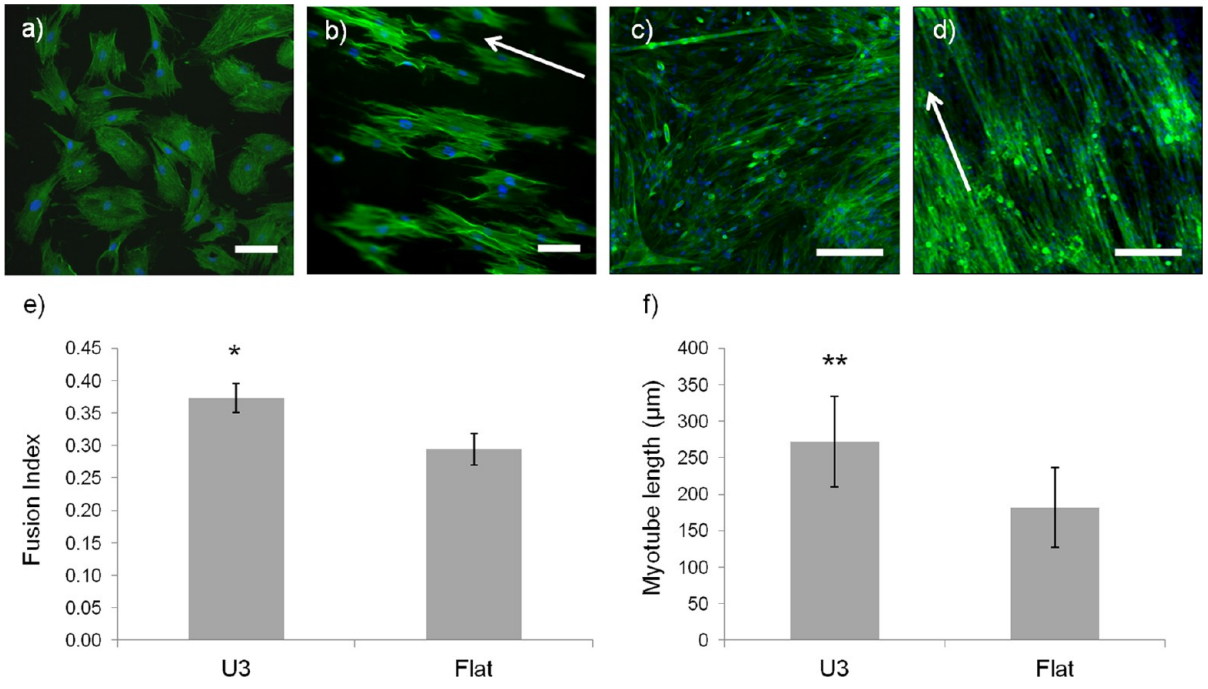

Figure 6. (a,b) nHDFs on flat (a) and U3 (b) PEDOT:PSS substrates, 24 h after seeding. Fluorescent images show F-actin (in green) and nuclei (in blue). Scale bar = 50 μm. (c,d) Fluorescence images of myotubes on control flat substrates (c) and U3 samples (d), supported by human fibroblasts feeder layer. Scale bar = 200 μm. A white arrow in (b,d) shows the direction of the nanowrinkles. Fusion Index (e) and myotube length (f) after 7 days of differentiation, with fibroblasts as feeder layer. * = $p < 0.05$, ** = $p < 0.01$.

(Supporting Information, Figure S5.a) and a clear cell anisotropy on nanowrinkled samples (Supporting Information, Figure S5.b).

Cell Differentiation and Myotube Alignment. As a first attempt, we tried to differentiate C2C12 cultured on U3 and flat control samples, by switching the culture medium to low-serum medium for 7 days. We succeeded in obtaining elongated multinucleated syncytia, randomly oriented in the case of flat control substrates and well aligned along nanowrinkle direction in the case of U3 samples (Supporting Information, Figure S6). However, myotube length and width remained quite limited, and few myotubes included more than 2 cell nuclei on both substrates, suggesting a low fusion index and therefore a reduced differentiation capability. This can be attributed to several factors, among which a reduced absorption of Fn and/or serum proteins on PEDOT:PSS substrates and a unfavorable PEDOT:PSS surface chemistry for C2C12 differentiation.

To improve cell differentiation, we adopted a strategy based on a co-culture of C2C12 cells and nHDFs, using fibroblasts as feeder layer for muscle development. This had a double aim. The former was to provide C2C12 cells with a soft fibroblast layer (~14 kPa), approaching the optimal substrate stiffness value needed for muscle differentiation.[47] The latter concerned the cytokines produced by fibroblasts during the co-culture, that further enhanced C2C12 differentiation. From previous literature reports, it is known that a feeder layer of nHDFs enhances C2C12 differentiation toward mature skeletal muscle.[48] First of all, we confirmed that also nHDFs resulted randomly oriented on flat control substrates (Figure 6a) and strongly aligned along the wrinkle axis on U3 samples, with actin fibers clearly elongated in the direction of wrinkle alignment (Figure 6b). Thanks to the co-culture-based approach, we obtained long and multinucleated myotubes after 7 days of differentiation (Figure 6c,d). Interestingly, myotube alignment along the nanowrinkle axis was maintained even in the presence of the fibroblast feeder layer (Figure 6d), while flat control samples were characterized again by randomly oriented myotubes (Figure 6c). Some myotube-related parameters are reported, in particular concerning fusion index (Figure 6e), and myotube length (Figure 6f). Results show that nanowrinkled substrates provided a higher differentiative stimulus in comparison with flat controls, promoting multinucleated and elongated myotube formation. We assume that the majority of C2C12 cells grew and then differentiated directly on top of the fibroblasts. A confluent layer of C2C12 cells (Supporting Information, Figure S5.a,b) was actually directly seeded on top of nHDFs already covering a significant fraction of the substrate area (Figure 6a,b).

Patterned Surfaces. To develop dynamic patterns for cell culturing and to combine this feature with the topographical features of the wrinkled substrates it is important to achieve a tunable control of surface conductivity in situ. Indeed, this capability is very important to electrically address selected areas of the substrate, to exploit in a controlled way the electroactive properties of conducting polymers, or simply to apply electric fields to the cultured cells. Controlled and reversible oxidation/reduction of PEDOT:PSS and other conducting polymers in situ can direct cell adhesion or even influence the cell's fate, as recently evidenced in some studies.[28,49−51] As an example, smart Petri dishes based on PEDOT:Tosylate have been developed to enable cell density control on their surface.[28] Polypyrrole (PPy) also was tailored to modulate survival and maintenance of rat fetal neural stem cells (NSCs); electrical reduction of PPy doped with different counterions caused alterations in polymer surface properties, thus leading to impaired cell viability.[50] Such studies suggest that these effects are caused by modifications in Fn adsorption and conforma-

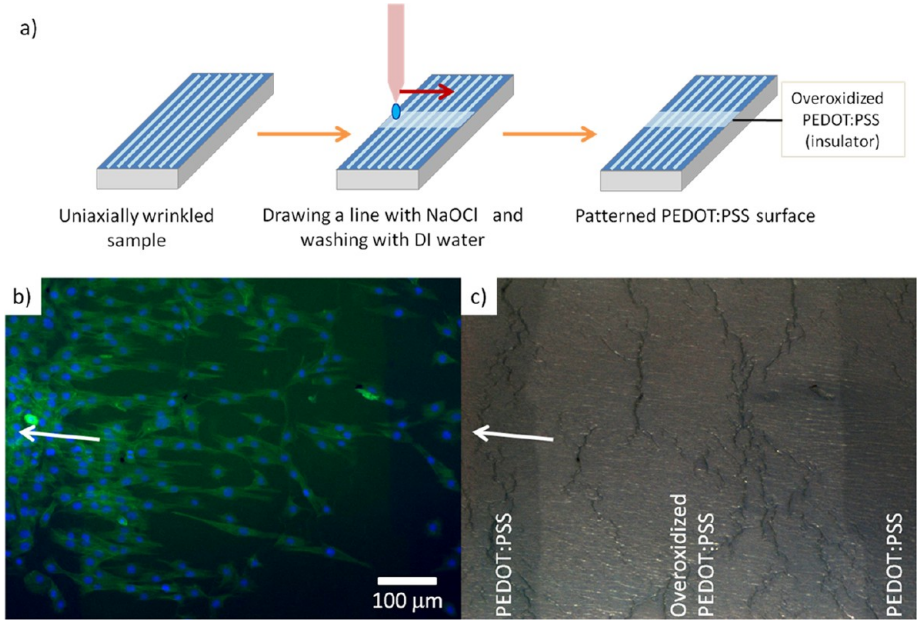

Figure 7. Patterning of conductive properties of wrinkled substrates. (a) Schematic drawing of the steps performed for achieving patterning of the PEDOT:PSS layer in uniaxially wrinkled samples. Localized overoxidation of PEDOT:PSS caused the loss of its conductive properties. Fluorescence (b) and bright field (c) images of C2C12 cells cultured for 24 h on a patterned U3p sample (initial cell density: 20,000 cells/cm^2) showing cell adhesion on the overoxidized region. Differences between pristine PEDOT:PSS and overoxidized regions are due to the increase of PEDOT:PSS optical transparency after the overoxidation process.

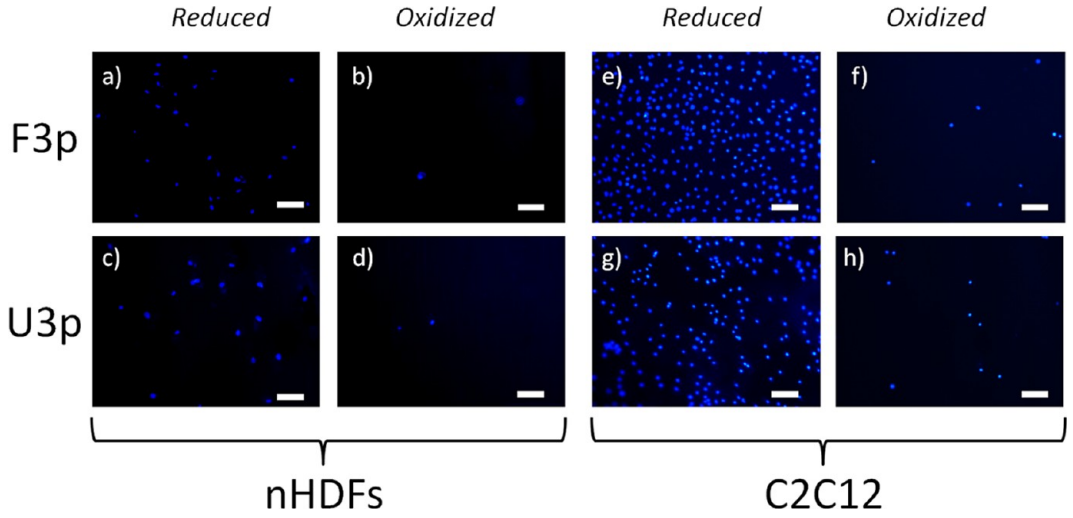

Figure 8. Cells cultivated in biased F3p and U3p substrates. Fluorescent images show nuclei (in blue) of nHDFs (a–d, initial cell density: 10,000 cells/cm^2) and C2C12 cells (e–h, initial cell density: 100,000 cells/cm^2) on the biased PEDOT:PSS surface after 24 h culture. For each cell type: left, reduced surface; right, oxidized surface. Scale bar = 100 μm.

tion,[51] known to be very important factors for the guidance of many cell functions. This hypothesis was further confirmed in a very recent work focused on assessing Fn conformation on PEDOT:Tosylate surface by using Förster Resonance Energy Transfer (FRET) imaging and developing a device allowing for precise control of protein conformation over macroscopic areas.[52]

We realized an easy patterning of the conductive properties of U3 wrinkled samples, by locally overoxidizing PEDOT:PSS. A schematic drawing depicting the patterning process and some pictures of cells adhering on patterned samples are reported in Figure 7. The patterning was based on local irreversible overoxidation of PEDOT:PSS by sodium hypochlorite, acting as oxidizing agent. This irreversible deactivation process is known to overoxidize PEDOT causing the loss of conductive properties (the oxidized region become insulating), as well as a color change from blue to transparent.[53] We fabricated a simple pattern to test the feasibility of the proposed approach. We drew an insulating gap on samples U3 in the form of a deactivated line with width ~500 μm, separating the surface into two individually addressable electrodes. It is important to note that the patterning process with sodium hypochlorite did not affect the topography of the wrinkled samples, as assessed by AFM measurements performed in the overoxidized region (data not shown), because patterning was performed after the shrinking process. The tested samples were patterned by simply placing filter paper strips soaked in the oxidizer solution, but this kind of patterning can be extended to other techniques,

such as inkjet[53] or microcontact printing,[54] allowing the fabrication of more complicated patterns and a significant reduction of size and resolution of the patterned features to some tens of micrometer or even to few micrometers. Patterned samples (U3p) and flat patterned control samples (F3p) showed uniform Fn coating, as evidenced in Supporting Information, Figure S7, with no differences observed in the deactivated region in comparison with pristine PEDOT:PSS areas. Figure 7b shows a fluorescence image of C2C12 cells cultured on both the deactivated and the pristine regions: the overoxidized area is identified as the central light-gray region in the corresponding bright-field picture (Figure 7c). Qualitative images and quantitative analyses (not shown) revealed no significant differences concerning cell adhesion and orientation between cells cultured on overoxidized and nonpatterned regions, on U3 samples.

Electrical Patterning of Cells on Conductive Substrates. As a first proof of concept of cell patterning controlled by electrochemical modulation of surface properties, we studied how the redox state of PEDOT:PSS can be used to control nHDFs and C2C12 cell adhesion by employing a bias voltage to switch the surface of patterned U3p and F3p samples.

Both nHDFs and C2C12 cells were deeply affected by the different redox state of the two regions of biased F3p and U3p substrates. nHDFs adhesion was significantly higher on reduced portion in comparison with oxidized one (Figure 8a–d), for both F3p and U3p samples. Similar results were obtained with C2C12 cells (Figure 8e–h), with more nuclei observed on reduced F3p and U3p portions, in comparison with the oxidized counterparts. These outcomes are consistent with previous literature findings, obtained for epithelial cells cultured for 24 h, under the same electrical conditions, on reduced and oxidized PEDOT:Tosylate substrates.[49]

The capability of deeply affecting the adhesion properties of both cell types (fibroblasts and muscle cells) by exploiting the conductive features of the tested substrates opens new avenues for the fabrication of smart engineered substrates able to finely pattern complex cell co-cultures and to determine at the same time their specific preferential orientation, by means of wrinkle-based topographical cues.

As a perspective, further detailed studies on Fn absorption and on cell adhesion and proliferation, both on the deactivated region and on active PEDOT:PSS when changing its redox state, would be beneficial for assessing the potential of these smart substrates for cell-based applications.

CONCLUSIONS

A novel approach was presented for producing anisotropic topographical cues at the micro- and nanoscale on conductive PEDOT:PSS surfaces, to be used as smart scaffolds for functional cell alignment and electrical stimulation.

Self-organizing multiscale hierarchical wrinkle formation over large areas (several cm^2) was obtained; the formed wrinkles were very robust and strongly adhered to the substrate. In the case of uniaxial wrinkles, a very well aligned quasi-periodic structure was formed, with different populations of wavelengths ranging from submicrometric to 10–20 μm, depending on PEDOT:PSS thickness. A key feature of this method relies on the fact that the employed materials (i.e., prestressed polystyrene and PEDOT:PSS) and process allowed for rapid and cost-effective production of highly ordered wrinkled surfaces in an all-organic smart scaffold, with the added benefits of being conductive and biocompatible.

Adhesion and proliferation of C2C12 murine skeletal muscle cells on uniaxially wrinkled samples were evaluated, comparing different topographies. The cells preferentially adhered and anisotropically aligned on low and narrow ridges (1.5 μm height) rather than on higher and wider ones (2.5 μm height). Moreover, C2C12 differentiation, with the formation of multinucleated and elongated myotubes, was achieved by co-culturing C2C12 cells with a fibroblast feeder layer on microwrinkled substrates. In this case, fibroblasts first adhered and aligned on the wrinkled structures and were then able to transfer a preferential alignment direction to C2C12 cells, subsequently seeded on the same substrate, thus allowing to obtain differentiated and anisotropically aligned skeletal myotubes.

Finally, to combine tunable control of surface conductivity in situ with the topographical features of the wrinkled substrates, a method for patterning the conductive properties of the wrinkled surfaces by locally overoxidizing PEDOT:PSS was presented. Fibronectin adsorption and cell adhesion on wrinkled substrates with a simple line pattern was tested, to demonstrate the feasibility of the proposed approach. Such patterning process could allow, for example, to fabricate electrodes for applying electric fields to cells during culture. Electric fields would be beneficial for the contraction of aligned myotubes on nanowrinkles, envisioning the development and the application of novel smart BioMEMS. Furthermore, this achievement could pave the way for the development of dynamic surface patterning by exploiting the electroactive properties of the conducting polymer PEDOT:PSS. Cell patterning controlled by electrochemical modulation of surface properties, was demonstrated, controlling nHDFs and C2C12 cell adhesion by employing a bias voltage to switch the redox state of adjacent electrodes on patterned flat and uniaxially wrinkled samples. Reduced polymer promoted cell adhesion in contrast to the oxidized one for both cells types and on both studied topographies.

ASSOCIATED CONTENT

Supporting Information

Seven additional figures (Figures S1–S7) with details on pictures of actual samples, surface topography of Polyshrink without coating before and after shrinking, topography of biaxially wrinkled samples, effect on cell culture of using different concentrations of fibronectin, cell alignment with high cell density seeding, differentiation properties of C2C12 cells without fibroblasts feeder layer on uniaxially wrinkled samples, fibronectin coating of wrinkled and patterned samples. This material is available free of charge via the Internet at http://pubs.acs.org.

AUTHOR INFORMATION

Corresponding Author

*E-mail: francesco.greco@iit.it.

Notes

The authors declare no competing financial interest.

ACKNOWLEDGMENTS

Mr. Danilo Franco is acknowledged for his precious help in materials selection and supply. This work was supported in part by JFE (The Japanese Foundation for Research and Promotion of Endoscopy) Grant (T.F.). F.G. and T.F. contributed equally as lead authors.

REFERENCES

(1) Bettinger, C. J.; Langer, R.; Borenstein, J. T. *Angew. Chem., Int. Ed.* **2009**, *48*, 5406−5415.
(2) Watt, F. M.; Jordan, P. W.; Oneill, C. H. *Proc. Natl. Acad. Sci. U. S. A.* **1988**, *85*, 5576−5580.
(3) Dalby, M. J.; Riehle, M. O.; Yarwood, S. J.; Wilkinson, C. D. W.; Curtis, A. S. G. *Exp. Cell Res.* **2003**, *284*, 274−282.
(4) Kim, D. H.; Lipke, E. A.; Kim, P.; Cheong, R.; Thompson, S.; Delannoy, M.; Suh, K. Y.; Tung, L.; Levchenko, A. *Proc. Natl. Acad. Sci. U. S. A.* **2010**, *107*, 565−570.
(5) Nathan, A. S.; Baker, B. M.; Nerurkar, N. L.; Mauck, R. L. *Acta Biomater.* **2011**, *7*, 57−66.
(6) Charest, J. L.; Eliason, M. T.; Garcia, A. J.; King, W. P. *Biomaterials* **2006**, *27*, 2487−2494.
(7) Flemming, R. G.; Murphy, C. J.; Abrams, G. A.; Goodman, S. L.; Nealey, P. F. *Biomaterials* **1999**, *20*, 573−588.
(8) Chen, C. S.; Mrksich, M.; Huang, S.; Whitesides, G. M.; Ingber, D. E. *Science* **1997**, *276*, 1425−1428.
(9) Marklein, R. A.; Burdick, J. A. *Adv. Mater.* **2010**, *22*, 175−189.
(10) Guillame-Gentil, O.; Semenov, O.; Roca, A. S.; Groth, T.; Zahn, R.; Vörös, J.; Zenobi-Wong, M. *Adv. Mater.* **2010**, *22*, 5443−5462.
(11) Bettinger, C. J.; Orrick, B.; Misra, A.; Langer, R.; Borenstein, J. T. *Biomaterials* **2006**, *27*, 2558−2565.
(12) Bruckner, P. *Cell Tissue Res.* **2010**, *339*, 7−18.
(13) Jiang, X.; Takayama, S.; Qian, X.; Ostuni, E.; Wu, H.; Bowden, N.; LeDuc, P.; Ingber, D. E.; Whitesides, G. M. *Langmuir* **2002**, *18*, 3273−3280.
(14) Engelmayr, G. C.; Cheng, M.; Bettinger, C. J.; Borenstein, J. T.; Langer, R.; Freed, L. E. *Nat. Mater.* **2008**, *7*, 1003−1010.
(15) Dalby, M. J.; Gadegaard, N.; Tare, R.; Andar, A.; Riehle, M. O.; Herzyk, P.; Wilkinson, C. D. W.; Oreffo, R. O. C. *Nat. Mater.* **2007**, *6*, 997−1003.
(16) Chung, J. Y.; Nolte, A. J.; Stafford, C. M. *Adv. Mater.* **2011**, *23*, 349−368.
(17) Genzer, J.; Groenewold, J. *Soft Matter* **2006**, *2*, 310−323.
(18) Efimenko, K.; Rackaitis, M.; Manias, E.; Vaziri, A.; Mahadevan, L.; Genzer, J. *Nat. Mater.* **2005**, *4*, 293−297.
(19) Lin, P.-C.; Yang, S. *Appl. Phys. Lett.* **2007**, *90*, 241903.
(20) Yin, J.; Yagüe, J. L.; Eggenspieler, D.; Gleason, K. K.; Boyce, M. C. *Adv. Mater.* **2012**, *24*, 5441−5446.
(21) Bowden, N.; Brittain, S.; Evans, A. G.; Hutchinson, J. W.; Whitesides, G. M. *Nature* **1998**, *393*, 146−149.
(22) Fu, C. C.; Grimes, A.; Long, M.; Ferri, C. G. L.; Rich, B. D.; Ghosh, S.; Lee, L. P.; Gopinathan, A.; Khine, M. *Adv. Mater.* **2009**, *21*, 4472.
(23) Chen, A.; Lieu, D. K.; Freschauf, L.; Lew, V.; Sharma, H.; Wang, J.; Nguyen, D.; Karakikes, I.; Hajjar, R. J.; Gopinathan, A.; Botvinick, E.; Fowlkes, C. C.; Li, R. A.; Khine, M. *Adv. Mater.* **2011**, *23*, 5785−5791.
(24) Guvendiren, M.; Burdick, J. A. *Biomaterials* **2010**, *31*, 6511−6518.
(25) Berggren, M.; Richter-Dahlfors, A. *Adv. Mater.* **2007**, *19*, 3201−3213.
(26) Guimard, N. K.; Gomez, N.; Schmidt, C. E. *Prog. Polym. Sci.* **2007**, *32*, 876−921.
(27) Isaksson, J.; Kjäll, P.; Nilsson, D.; Robinson, N.; Berggren, M.; Richter-Dahlfors, A. *Nat. Mater.* **2007**, *6*, 673−679.
(28) Saltó, C.; Saindon, E.; Bolin, M.; Kanciurzewska, A.; Fahlman, M.; Jager, E. W. H.; Tengvall, P.; Arenas, E.; Berggren, M. *Langmuir* **2008**, *24*, 14133−14138.
(29) Bolin, M. H.; Svennersten, K.; Wang, X.; Chronakis, I. S.; Richter-Dahlfors, A.; Jager, E. W. H.; Berggren, M. *Sens. Actuators, B* **2009**, *142*, 451−456.
(30) Smela, E. *Adv. Mater.* **2003**, *15*, 481−494.
(31) Ravichandran, R.; Sundarrajan, S.; Venugopal, J. R.; Mukherjee, S.; Ramakrishna, S. *J. R. Soc., Interface* **2010**, *7*, S559−S579.
(32) Mawad, D.; Stewart, E.; Officer, D. L.; Romeo, T.; Wagner, P.; Wagner, K.; Wallace, G. G. *Adv. Funct. Mater.* **2012**, *22*, 2692−2699.
(33) Schmidt, C. E.; Shastri, V. R.; Vacanti, J. P.; Langer, R. *Proc. Natl. Acad. Sci. U. S. A.* **1997**, *94*, 8948−8953.
(34) Bendrea, A.-D.; Cianga, L.; Cianga, I. *J. Biomater. Appl.* **2011**, *26*, 3−84.
(35) Le, D. M.; Kulangara, K.; Adler, A. F.; Leong, K. W.; Ashby, V. S. *Adv. Mater.* **2011**, *23*, 3278−3283.
(36) Davis, K. A.; Burke, K. A.; Mather, P. T.; Henderson, J. H. *Biomaterials* **2011**, *32*, 2285−2293.
(37) Kim, J.; Yoon, J.; Hayward, R. C. *Nat. Mater.* **2010**, *9*, 159−164.
(38) Greco, F.; Zucca, A.; Taccola, S.; Menciassi, A.; Fujie, T.; Haniuda, H.; Takeoka, S.; Dario, P.; Mattoli, V. *Soft Matter* **2011**, *7*, 10642−10650.
(39) Ricotti, L.; Taccola, S.; Bernardeschi, I.; Pensabene, V.; Dario, P.; Menciassi, A. *Biomed. Mater.* **2011**, *6*, 031001.
(40) Kaliappan, S. K.; Cappella, B. *Polymer* **2005**, *46*, 11416−11423.
(41) Toworfe, G. K.; Composto, R. J.; Adams, C. S.; Shapiro, I. M.; Ducheyne, P. *J. Biomed. Mater. Res., Part A* **2004**, *71A*, 449−461.
(42) Gingras, J.; Rioux, R. M.; Cuvelier, D.; Geisse, N. A.; Lichtman, J. W.; Whitesides, G. M.; Mahadevan, L.; Sanes, J. R. *Biophys. J.* **2009**, *97*, 2771−2779.
(43) Wang, P.-Y.; Yu, H.-T.; Tsai, W.-B. *Biotechnol. Bioeng.* **2010**, *106*, 285−294.
(44) Clark, P.; Dunn, G. A.; Knibbs, A.; Peckham, M. *Int. J. Biochem. Cell Biol.* **2002**, *34*, 816−825.
(45) Ciofani, G.; Ricotti, L.; Mattoli, V. *Biomed. Microdevices* **2011**, *13*, 255−266.
(46) Lam, M. T.; Sim, S.; Zhu, X.; Takayama, S. *Biomaterials* **2006**, *27*, 4340−4347.
(47) Engler, A. J.; Griffin, M. A.; Sen, S.; Bönnemann, C. G.; Sweeney, H. L.; Discher, D. E. *J. Cell Biol.* **2004**, *166*, 877−887.
(48) Cooper, S. T.; Maxwell, A. L.; Kizana, E.; Ghoddusi, M.; Hardeman, E. C.; Alexander, I. E.; Allen, D. G.; North, K. N. *Cell Motil. Cytoskeleton* **2004**, *58*, 200−211.
(49) Svennersten, K.; Bolin, M. H.; Jager, E. W. H.; Berggren, M.; Richter-Dahlfors, A. *Biomaterials* **2009**, *30*, 6257−6264.
(50) Lundin, V.; Herland, A.; Berggren, M.; Jager, E. W. H.; Teixeira, A. I. *PLoS ONE* **2011**, *6*, e18624.
(51) Molino, P. J.; Higgins, M. J.; Innis, P. C.; Kapsa, R. M.; Wallace, G. G. *Langmuir* **2012**, *28*, 8433−8445.
(52) Wan, A. M. D.; Schur, R. M.; Ober, C. K.; Fischbach, C.; Gourdon, D.; Malliaras, G. G. *Adv. Mater.* **2012**, *24*, 2501−2505.
(53) Yoshioka, Y.; Calvert, P. D.; Jabbour, G. E. *Macromol. Rapid Commun.* **2005**, *26*, 238−246.
(54) Hansen, T. S.; West, K.; Hassager, O.; Larsen, N. B. *Adv. Mater.* **2007**, *19*, 3261−3265.